


Propagation of rays in 2D and 3D waveguides: A stability analysis with Lyapunov and reversibility fast indicators

Cite as: Chaos **31**, 043138 (2021); <https://doi.org/10.1063/5.0043782>

Submitted: 11 January 2021 . Accepted: 02 April 2021 . Published Online: 29 April 2021

 G. Gradoni,  F. Panichi, and  G. Turchetti

COLLECTIONS

 This paper was selected as Featured



View Online



Export Citation



CrossMark

ARTICLES YOU MAY BE INTERESTED IN

Data-driven modeling of nonlinear traveling waves

Chaos: An Interdisciplinary Journal of Nonlinear Science **31**, 043128 (2021); <https://doi.org/10.1063/5.0043255>

Quasi-objective coherent structure diagnostics from single trajectories

Chaos: An Interdisciplinary Journal of Nonlinear Science **31**, 043131 (2021); <https://doi.org/10.1063/5.0044151>

A criterion for mixed dynamics in two-dimensional reversible maps

Chaos: An Interdisciplinary Journal of Nonlinear Science **31**, 043133 (2021); <https://doi.org/10.1063/5.0040444>

Scilight

Summaries of the latest breakthroughs
in the physical sciences



Propagation of rays in 2D and 3D waveguides: A stability analysis with Lyapunov and reversibility fast indicators

Cite as: Chaos 31, 043138 (2021); doi: 10.1063/5.0043782

Submitted: 11 January 2021 · Accepted: 2 April 2021 ·

Published Online: 29 April 2021



View Online



Export Citation



CrossMark

G. Gradoni,^{1,a),b)}  F. Panichi,^{2,b)}  and G. Turchetti^{3,b)} 

AFFILIATIONS

¹School of Mathematical Sciences and Department of Electrical and Electronic Engineering, University of Nottingham, University Park, NG72RD Nottingham, United Kingdom

²Numerical Algorithms Group Ltd, Portland Street 53, M1-3LD Manchester, United Kingdom

³Department of Physics and Astronomy, Alma Mater Studiorum, University of Bologna, Viale Berti Pichat 6/2, 40-127 Bologna, Italy and INDAM Gruppo Nazionale di Fisica Matematica, Piazzale Aldo Moro, 5, 00185 Roma, Italy

^{a)}Also at: Maxwell Centre, University of Cambridge, United Kingdom.

^{b)}Authors to whom correspondence should be addressed: gabriele.gradoni@nottingham.ac.uk; federico.panichi@studio.unibo.it; and giorgio.turchetti@unibo.it

ABSTRACT

Propagation of rays in 2D and 3D corrugated waveguides is performed in the general framework of stability indicators. The analysis of stability is based on the Lyapunov and reversibility error. It is found that the error growth follows a power law for regular orbits and an exponential law for chaotic orbits. A relation with the Shannon channel capacity is devised and an approximate scaling law found for the capacity increase with the corrugation depth.

Published under an exclusive license by AIP Publishing. <https://doi.org/10.1063/5.0043782>

We investigate the propagation of a ray in a 2D waveguide whose boundaries are two parallel horizontal lines with a periodic corrugation on the upper line. The reflection point abscissa on the lower line and the ray horizontal velocity component after reflection are the phase space coordinates and the map connecting two consecutive reflections is symplectic. The dynamic behavior is illustrated by the phase portraits, which show that the regions of chaotic motion increase with the corrugation amplitude. For a 3D waveguide, the 4D map connecting two consecutive reflections on the lower plane is symplectic, but its orbit cannot be examined by looking at the intersections with a 2D phase plane, since a continuous interpolation of the orbits is not available. In this case, the fast dynamic indicators allow to perform a stability analysis. For each point of a grid in a 2D phase plane, one computes the orbit for a chosen number of iterations and the corresponding value of the fast indicator, which is conveniently visualized using a color plot. After the fast Lyapunov indicator, many other indicators have been introduced. Our analysis is based on the Lyapunov error (LE) due to a small random initial displacement and the reversibility error occurring when the orbit is reversed in presence of a small additive noise [reversibility error (RE)]

or roundoff [modified reversibility error (REM)]. For integrable maps, the growth of LE and RE follows a power law and for quasi-integrable maps the same growth occurs close to a stable fixed point. More generally, the error growth follows a power law for regular orbits and an exponential law for chaotic orbits. Near the boundary between two invariant regions of regular and chaotic motion, we find sticky orbits for which the error grows first following a power law, possibly for long periods, switching to an exponential at later times. There is numerical evidence that REM grows as RE though with large fluctuations. The channel capacity is related to LE and the dependence of its phase space average on the corrugation amplitude is considered. Our indicators confirm their reliability for the stability analysis of the ray propagation in a 2D and 3D waveguide, providing a measure of the sensitivity of the orbits to initial conditions, noise, and roundoff.

I. INTRODUCTION

The equivalence between geometrical optics and mechanics was established in a variational form by the principles of Fermat and Maupertuis. If a ray propagates in a uniform medium with

a reflecting boundary, then the trajectory is the same as a particle freely moving and elastically colliding with the same boundary. As a consequence, a waveguide and a billiard are equivalent optical and mechanical systems.¹ Since the velocity of the particle does not change, we can assume that it has unit modulus, just as the ray velocity normalized to the speed of light. The trajectory is determined by the collision points and the velocity direction after the collision. The billiards with polygonal or smooth convex closed boundaries have been intensively investigated and the mathematical literature is very rich (see Refs. 2–6). The behavior of level spacing of quantum chaotic billiards was investigated^{7,8} and related to spectrum of random matrices.

We first consider the 2D waveguide whose boundary is a straight line and a corrugated parallel line. The trajectory is a polygonal line specified by the abscissa x of the reflection points on the straight line and the parallel component v_x of the velocity after reflection. The Fermat principle establishes that, given two points of abscissas x_1, x_2 on the lower straight line, the ray starting from x_1 , colliding once with the corrugated line, and reaching x_2 follows the path of minimal length and the collision is just a reflection. In addition, the ray minimal path length $h(x_1, x_2)$ is the generating function of the area preserving map M connecting two subsequent reflections on the straight line. A similar procedure allows us to obtain a symplectic map for the ray propagation in a 3D waveguide made of an horizontal plane and an upper parallel plane with a periodic corrugation. If the medium between the waveguide boundaries is not uniform, the piecewise linear path joining two consecutive reflection points on the lower line or plane is replaced by the geodesic with respect to the metric $n ds$, where n is the refraction index.

The transition from ordered to chaotic motion in 2D billiards and waveguides has been considered;^{9–11} the transport and diffusion properties have been extensively analyzed.^{12–18} The stability properties of the map depend on the corrugation amplitude. For the 2D waveguide, the phase portrait of the corresponding 2D map allows us to detect the regions of regular and chaotic motion. Finite time indicators such as the Fast Lyapunov Indicator (FLI)^{19,20} have been first proposed to analyze the orbital stability (see Appendix A).

Many other fast Lyapunov indicators were introduced. For an extensive list and numerical comparison for symplectic maps see.^{22,23}

Recently, the Lyapunov and reversibility errors have been introduced^{26,27} to measure the sensitivity of the orbits to a small random initial displacement and to a small additive noise along the orbit. The Lyapunov error (LE) and the reversibility error are simply related²⁸ so that the computation of RE does not require expensive Monte Carlo procedures. The relevant difference of LE with respect to previous variational indicators such as FLI, is that LE does not depend on the initial deviation vectors. A full set of Lyapunov error invariant indicators (LEIs), whose asymptotic behavior is related to the partial sums of the Lyapunov exponents, just as GALI,²¹ and which independent from the initial deviation vectors, has been introduced jointly with reversibility error invariant indicators (REIs).²⁹ The REIs are asymptotically governed by the partial sums of positive Lyapunov exponents. The logarithms of the last REI is the reversibility entropy, whose asymptotic behavior is governed by the sum of positive Lyapunov exponents, just as the Ruelle upper-bound to the measure theoretic entropy,²⁴ which is

related to the topological entropy, the information entropy, and the Kolmogorov–Sinai entropy.²⁵

The LE and RE grow following a power law, for the regular orbits of quasi-integrable symplectic maps as the previous variational indicators, exponentially for chaotic orbits. The reversibility error due to roundoff (REM) was first introduced in Ref. 30 and its features were examined in Ref. 31. For previous works on the round effect in the computation of orbits for Hamiltonian systems, see Ref. 32. Previous numerical investigations of Hamiltonian systems and symplectic maps confirm that LE grows linearly with oscillations (due to the loss of rotational symmetry when the coordinates are not normal) for regular orbits, whereas the growth of RE is almost oscillations free. Neglecting its large fluctuations REM is comparable with RE, even though no rigorous proof is available.

For the 3D waveguide, no direct inspection of the orbits is possible, since the section of the orbits of the symplectic 4D map with a 2D plane would require a continuous interpolation, available only when an interpolating Hamiltonian is known. Normal forms provide the interpolating Hamiltonian for quasi-integrable symplectic maps, but their recursive computation is possible just for polynomial maps, and, in addition, the interpolation is not exact due to the presence of a nonintegrable remainder. The variational indicators, computed for the orbits issued from the points of a regular grid in a 2D phase plane for the 4D map and visualized with a color plot, allow us to determine the stability properties just as for the 2D map. We have analyzed only LE and RE for a limited number of iterations. Indeed, as stated by Froeschlé *et al.*, the variational indicators as FLI computed for short times exhibit some dependency on the initial deviation vectors. Since LE, RE, and REM do not depend on the initial deviation vectors our choice is justified. A careful investigation of the sticky chaos, which requires longer orbits, and more extensive numerical exploration of the reflection maps based on the full set of invariant indicators LEI and REI and a comparison with the standard variational indicators, will be the object of a future work.

Only a few hundred iterations of the map are required to obtain a reliable stability picture, unless one is interested in the details of a small region. To obtain the analytic form of the tangent map is rather cumbersome for the 3D waveguide case. The shadow orbit method provides a simple, though less accurate, alternative, which consists in evaluating the orbits for initial conditions with small displacements along an orthogonal basis, which amounts to replace the partial derivatives with finite differences. For any initial condition, four additional evaluations of the orbit are required (two for the 2D map) in order to obtain LE and RE, whereas just one is required to compute REM.

We have analyzed a model of 2D waveguide for different values of the corrugation amplitude, showing that the LE, RE, and REM provide comparable results, which describe the orbits sensitivity to a small initial random displacement, to an additive noise along the orbit and to round off. For a model of 3D waveguide, the same error plots for initial conditions on 2D phase planes exhibit a similar behavior, though the structure is richer with respect to the 2D waveguide due to the presence of the Arnold web of resonances. The effectiveness of the proposed method, already experienced in celestial mechanics^{26,27} and beam dynamics³³ models, is confirmed in these examples of 2D and 3D waveguides.

This paper is organized as follows. In Sec. II, we present the variational derivation of the reflections map for a 2D waveguide. In Sec. III, the extension to the 3D waveguide is outlined. In Sec. IV, our dynamical indicators are defined and their basic properties are illustrated. In Secs. V and VI, the numerical results of these indicators show how the instability regions grow when the corrugation amplitude increases. In Sec. VII, the link between our indicators and the channel capacity is established and it is shown how its phase space average increases with the corrugation amplitude. Conclusions and perspectives are presented in Sec. VIII.

II. THE 2D WAVEGUIDE

Given two parallel reflecting lines $z = 0$ and $z = 1$ in the (x, z) plane, the light ray direction after each reflection on the lower line is the same being specified by the unit vector $\mathbf{v} = (x_x, v_x = \sqrt{1 - v_x^2})^T$, where T denotes the transpose of a matrix or a vector. The time τ between two reflections on the upper and lower line is given by $\tau v_x = 1$. We choose as phase space coordinates (x, v_x) so that the sequence of reflections (x_n, v_{x_n}) on the lower line is given by

$$\begin{aligned} v_{x_{n+1}} &= v_{x_n}, \\ x_{n+1} &= x_n + 2\tau v_{x_n} = x_n + \frac{2v_{x_n}}{\sqrt{1 - v_{x_n}^2}}. \end{aligned} \tag{1}$$

This map is integrable and area preserving. If we let $\mathbf{v} = (\cos \theta, \sin \theta)^T$, where $0 \leq \theta \leq \pi$, the map becomes

$$\theta_{n+1} = \theta_n \quad x_{n+1} = x_n + 2 \cot \theta_n, \tag{2}$$

and this preserves the measure $d\mu = \sin \theta \, dx d\theta$. If our phase space is a cylinder $\mathbb{T}([-\pi, \pi]) \times [-1, 1]$ rather than the infinite strip $\mathbb{R} \times [-1, 1]$, then x is an angle variable and v_x is an action variable.

The frequency $\Omega = 2v_x(1 - v_x^2)^{-1/2}$ diverges for $v_x \rightarrow \pm 1$ and the interpolating Hamiltonian is $H = -2\sqrt{1 - v_x^2}$. Since also Ω' diverges when $v_x \rightarrow \pm 1$, any perturbation renders the map chaotic as any perturbed integrable map near the separatrix where Ω vanishes but its derivative diverges. The 2D waveguide is obtained by corrugating the upper line according to

$$z = 1 + \varepsilon f(x), \tag{3}$$

where $f(x)$ is a periodic function of period 2π such that $f(x) > -1$ and $0 \leq \varepsilon \leq 1$. The curvilinear abscissa $s(x)$ of a point Q on the corrugated line of coordinates (x, z) is given by (4),

$$s(x) = \int_0^x \sqrt{1 + \varepsilon^2 f'^2(x')} \, dx'. \tag{4}$$

Consider a ray which starts from $P_0 = (x_0, 0)$ and reaches corrugated line at $Q = (x, z)$. After reflection, the ray reaches the x axis at the point $P_1 = (x_1, 0)$. Keeping P_0 and P_1 fixed and letting Q vary the path length H of the segments P_0Q and QP_1 is a function of $s(x)$

$$\begin{aligned} H(s) &= h(x_0, s) + h(x_1, s), \\ h(x_0, s) &= \sqrt{(x - x_0)^2 + (1 + \varepsilon f(x))^2}, \\ h(x_1, s) &= \sqrt{(x - x_1)^2 + (1 + \varepsilon f(x))^2}, \end{aligned} \tag{5}$$

where $x = x(s)$ is the inverse of the function $s = s(x)$ defined by (4). Referring to Fig. 1, we define ψ and ψ' the angles which the velocities \mathbf{v}_0 and \mathbf{v} of the incoming and outgoing ray at Q form with the tangent $\boldsymbol{\tau}$. The angles between the vectors $-\mathbf{v}_0$ and \mathbf{v} and the normal \mathbf{v} at Q are $\pi/2 - \psi$ and $\pi/2 - \psi'$. As a consequence

$$\begin{aligned} \mathbf{v}_0 &= \frac{(x - x_0, 1 + \varepsilon f(x))^T}{h(x_0, s)}, \quad \mathbf{v} = \frac{(x_1 - x, -1 - \varepsilon f(x))^T}{h(x_1, s)}, \\ \boldsymbol{\tau} &= \frac{(1, \varepsilon f'(x))^T}{\sqrt{1 + \varepsilon^2 f'^2(x)}}, \quad \mathbf{v}' = \frac{(\varepsilon f'(x), -1)^T}{\sqrt{1 + \varepsilon^2 f'^2(x)}}. \end{aligned} \tag{6}$$

We denote with \mathbf{v}_1 the velocity of the ray reflected at P_1 and with θ_0 and θ_1 the angles \mathbf{v}_0 and \mathbf{v}_1 form with the positive x axis [see (1)]. The derivatives of $h(x_0, s)$ and of $h(x_1, s)$ are given by

$$\begin{aligned} \frac{\partial}{\partial s} h(x_0, s) &= \frac{x - x_0 + (1 + \varepsilon f(x)) \varepsilon f'(x)}{h(x_0, s) \sqrt{1 + \varepsilon^2 f'^2(x)}} \\ &= \mathbf{v}_0 \cdot \boldsymbol{\tau} = \cos \psi, \\ \frac{\partial}{\partial x_0} h(x_0, s) &= \frac{x_0 - x}{h(x_0, s)} = -v_{x0} = -\cos \theta_0, \\ \frac{\partial}{\partial s} h(x_1, s) &= \frac{x - x_1 + (1 + \varepsilon f(x)) \varepsilon f'(x)}{h(x_1, s) \sqrt{1 + \varepsilon^2 f'^2(x)}} \\ &= -\mathbf{v} \cdot \boldsymbol{\tau} = -\cos \psi', \\ \frac{\partial}{\partial x_1} h(x_1, s) &= \frac{x_1 - x}{h(x_0, s)} = v_{x1} = \cos \theta_1. \end{aligned} \tag{7}$$

The stationary point H with respect to s , when x_0 and x_1 are kept fixed, is met for $s = s_*(x_1, x_2)$ where $\psi = \psi'$, which corresponds to the reflection condition. We introduce the function $F(x_0, x_1)$ equal to H at the stationary point $s = s_*(x_0, x_1)$ and compute its differential

$$\begin{aligned} F(x_0, x_1) &= h(x_0, x_1, s_*) + h(x_0, x_1, s_*), \\ dF(x_0, x_1) &= -v_{x0} \, dx_0 + v_{x1} \, dx_1. \end{aligned} \tag{8}$$

Equation (8) shows that $F(x_0, x_1)$ is the generating function of the canonical transformation M from (x_0, v_{x0}) to (x_1, v_{x1}) . After n iterations, the phase space point (x_n, v_{x_n}) is reached and is mapped into $(x_{n+1}, v_{x_{n+1}})$ by M . In the physical space, the ray issued from the point $P_n = (x_n, 0)$ with horizontal velocity v_{x_n} is reflected at $Q_n = (x_n, 1 + \varepsilon f(x_n))$ and reaches $P_{n+1} = (x_{n+1}, 0)$, where the horizontal velocity after reflection is $v_{x_{n+1}}$ (see Fig. 1).

In order to obtain the map, we first compute the time τ needed for the transit between P_n and Q_n . Then, we determine the horizontal component of the velocity $v_{x_{n+1}}$ of the ray outgoing from P_{n+1} , which is equal to v_{x_n} , where the velocity \mathbf{v}_* of the ray from Q_n to P_{n+1} is determined by the reflection condition $\mathbf{v}_* = \mathbf{v}_n - 2(\mathbf{v}_n \cdot \mathbf{v}_n)$ and the normal of the guide at Q_n is given by (6). Finally, $x_{n+1} - x_n$ is given by $v_{x_n} \tau + v_{x_{n+1}} \tau'$, where the transit time from τ' from Q_n

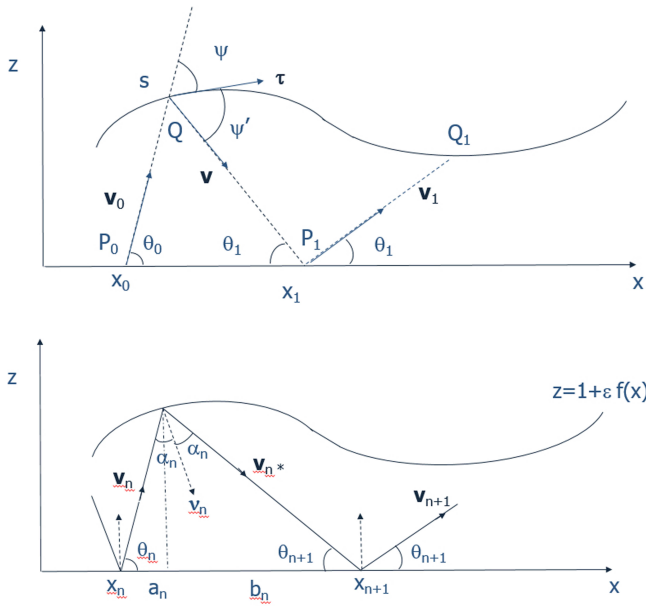


FIG. 1. Geometry of the reflections. On the right frame for $n = 0$, we have $\alpha_0 = \pi/2 - \psi$, where ψ is defined on the left frame.

to P_{n+1} is given by $v_{zn+1} \tau' = v_{zn} \tau$,

$$\begin{aligned}
 v_{zn} \tau &= 1 + \varepsilon f(x_n + \tau v_{xn}), \quad v_{zn} = \sqrt{1 - v_{xn}^2}, \\
 v_{xn+1} &= v_{xn} - 2v_x(\mathbf{v} \cdot \mathbf{v}_n) \\
 &= v_{xn} - 2 \frac{\varepsilon^2 f'^2 v_{xn} - \varepsilon f' v_{zn}}{1 + \varepsilon^2 f'^2}, \\
 f' &= f'(x_n + \tau v_{xn}), \\
 x_{n+1} &= x_n + \tau \left(v_{xn} + v_{xn+1} \frac{v_{zn}}{v_{zn+1}} \right), \\
 v_{zn+1} &= \sqrt{1 - v_{xn+1}^2}.
 \end{aligned}
 \tag{9}$$

The map $(x_{n+1}, v_{xn+1}) = M(x_n, v_{xn})$ is symplectic since it is implicitly defined by the generating function $F(x_n, x_{n+1})$ according to $v_{xn} = -\partial F/\partial x_n$ and $v_{xn+1} = \partial F/\partial x_{n+1}$. The computation of the tangent map is given in [Appendix B](#).

III. THE 3D WAVEGUIDE

In this case, we consider two planes $z = 0$ and $z = 1$ and the ray velocity is the unit vector \mathbf{v} , which can be written in Cartesian coordinates according to

$$\mathbf{v} = (v_x, v_y, v_z) \quad v_z = \sqrt{1 - v_x^2 - v_y^2}. \tag{10}$$

With \mathbf{v} , we denote the velocity of the ray reflected by the lower plane $z = 0$ so that $v_z > 0$. The time τ between a reflection on the lower and upper plane is $\tau v_z = 1$ so that, choosing (x, y, v_x, v_y) as phase

space coordinates, the map between two consecutive reflections reads

$$\begin{aligned}
 v_{xn+1} &= v_{xn}, \\
 v_{yn+1} &= v_{yn}, \\
 x_{n+1} &= x_n + 2\tau v_{xn} = x_n + 2 \frac{v_{xn}}{v_{zn}}, \\
 y_{n+1} &= y_n + 2\tau v_{yn} = y_n + 2 \frac{v_{yn}}{v_{zn}}.
 \end{aligned}
 \tag{11}$$

If the map is defined on $\mathbb{T}^2([-\pi, \pi]) \times [-1, 1]^2$, then v_x and v_y are the action variables and the interpolating Hamiltonian is $H = -2\sqrt{1 - v_x^2 - v_y^2}$. In the 3D waveguide, the plane $z = 1$ is corrugated, namely, it is replaced by the surface

$$z = z(x, y) = 1 + \varepsilon f(x, y), \tag{12}$$

where $f(x, y)$ is a periodic function in x and y with period 2π and $f > -1$ with $0 < \varepsilon < 1$. As a consequence, the map describing the rays propagation can be defined on $\mathbb{T}^2([-\pi, \pi]) \times [-1, 1]^2$. As in the 2D case, we consider the sequence of points $P_0, P_1, \dots, P_n, \dots$ on the $z = 0$ plane. We denote by Q_n the point on the upper corrugated plane hit by the ray issued from P_n , which after reflection reaches the $z = 0$ plane at P_{n+1} . The sequence points $P_0, P_1, \dots, P_n, \dots$ on the torus \mathbb{T}^2 is simply obtained taking the modulus with respect to 2π so that $(x'_n, y'_n) \in [-\pi, \pi]$. Letting $\mathbf{v}(x, y)$ be the normal at the corrugated surface at the reflection point $Q = (x, y, z = 1 + f(x, y))$, which explicitly reads as follows:

$$\mathbf{v}(x, y) = \frac{(\varepsilon f_x, \varepsilon f_y, -1)^T}{\sqrt{1 + \varepsilon^2(f_x^2 + f_y^2)}}. \tag{13}$$

The map $(x_{n+1}, y_{n+1}, v_{xn+1}, v_{yn+1}) = M(x_n, y_n, v_{xn}, v_{yn})$ specifying the ray trajectory is given by

$$\begin{aligned}
 \tau v_{zn} &= 1 + \varepsilon f(x_n + \tau v_{xn}, y_n + \tau v_{yn}), \\
 v_{zn} &= \sqrt{1 - v_{xn}^2 - v_{yn}^2}, \\
 v_{xn+1} &= v_{xn} - 2v_x(\mathbf{v} \cdot \mathbf{v}_n), \quad \mathbf{v} = \mathbf{v}(x_n + \tau v_{xn}, y_n + \tau v_{yn}), \\
 v_{yn+1} &= v_{yn} - 2v_y(\mathbf{v} \cdot \mathbf{v}_n), \\
 x_{n+1} &= x_n + \tau \left(v_{xn} + v_{xn+1} \frac{v_{zn}}{v_{zn+1}} \right), \\
 y_{n+1} &= y_n + \tau \left(v_{yn} + v_{yn+1} \frac{v_{zn}}{v_{zn+1}} \right), \\
 v_{zn+1} &= \sqrt{1 - v_{xn+1}^2 - v_{yn+1}^2}.
 \end{aligned}
 \tag{14}$$

The first equation implicitly defines the propagation time τ from P_n to Q_n , the remaining equations define the map M which is symplectic. Indeed starting from the Fermat variational principle, it is shown in [Appendix C](#) that this map is obtained from a generating function $F(x_n, y_n, x_{n+1}, y_{n+1})$. We do not quote in this case the expression of the tangent map since it is rather involved.

IV. DYNAMICAL INDICATORS

We will present a numerical analysis of the 2D and 4D symplectic maps whose orbits describe the propagation of a ray in a 2D and 3D periodic waveguide. The stability analysis is intended to discriminate the regions of regular and chaotic motions using the recently introduced fast stability indicators, denominated Lyapunov and Reversibility error. The first one is closely related to fast Lyapunov indicator first proposed to analyze the growth of a small initial displacement. We shall not present a comparison with other fast indicators, because it has been performed for other models and since our indicators are independent from the initial displacement.

A. Lyapunov error

For a symplectic map in a phase space of dimension $2d$ map, the Lyapunov error (LE) describes the growth of an initial random displacement $\varepsilon \xi$, where $\xi \in \mathbb{R}^{2d}$ is a random vector with zero mean and unit variance

$$\langle \xi \rangle = 0, \quad \langle \xi \xi^T \rangle = \mathbf{I} \quad (15)$$

in the zero amplitude limit $\varepsilon \rightarrow 0$. Denoting with Ξ_n the random displacement after n iteration and with $DM(x)$ the tangent map

$$\begin{aligned} \Xi_n(\mathbf{x}) &= \lim_{\varepsilon \rightarrow 0} \frac{M^n(\mathbf{x} + \varepsilon \xi) - M^n(\mathbf{x})}{\varepsilon} = L_n(\mathbf{x}) \xi, \\ L_n(\mathbf{x}) &= DM^n(\mathbf{x}) = DM(\mathbf{x}_{n-1}) L_{n-1}(\mathbf{x}). \end{aligned} \quad (16)$$

The square of the Lyapunov error $E_{L_n}(\mathbf{x})$ is defined as the variance of the random vector Ξ_n or the trace of its covariance matrix

$$E_{L_n}^2(\mathbf{x}) = \langle \Xi_n \cdot \Xi_n \rangle = \text{Tr}(\Sigma_n^2), \quad \Sigma_n^2 = \langle \Xi_n \Xi_n^T \rangle = L_n L_n^T. \quad (17)$$

We might define the error $E_{L_n}(\mathbf{x}, \eta)$ for a given initial displacement $\varepsilon \eta$ with $\|\eta\| = 1$, when $\varepsilon \rightarrow 0$. Its logarithm is just the fast Lyapunov indicator. We observe that letting \mathbf{e}_j be any orthonormal base the sum of $E_{L_n}^2(\mathbf{x}, \mathbf{e}_j)$ extended to all the vectors of base is equal to $E_{L_n}^2(\mathbf{x})$. Our definition is independent from the initial displacement. An expression for the Lyapunov error equivalent to (17) is given by

$$E_{L_n}^2(\mathbf{x}) = \text{Tr}(L_n^T(\mathbf{x}) L_n(\mathbf{x})) = \text{Tr}\left((DM^n(\mathbf{x}))^T DM^n(\mathbf{x})\right). \quad (18)$$

The stability analysis is performed by fixing n and observing the change of E_{L_n} when \mathbf{x} varies on a 2D phase plane (or a 2D manifold). Oseledet theorem³⁴ states that if \mathbf{x} belongs to an ergodic component, then $(L_n^T L_n)^{1/2n}$ has a limit $W e^\Lambda W^T$ independent from \mathbf{x} , where W is an orthogonal matrix, Λ is diagonal and its entries $\lambda_1 \geq \lambda_2 \geq \dots \geq \lambda_{2d}$ are the Lyapunov exponents with $\lambda_{d+k} = -\lambda_{d-k+1}$ and $\lambda_k \geq 0$ for $1 \leq k \leq d$. As a consequence, asymptotically $E_{L_n}^2 \simeq e^{2n\lambda_1} + e^{2n\lambda_2} + \dots + e^{2n\lambda_{2d}} \simeq e^{2n\lambda_1}$ and more rigorously $\lim_{n \rightarrow \infty} (E_{L_n})^{1/n} = \lambda_1$. However, we are not interested in the $n \rightarrow \infty$ limit but rather on the dependence on \mathbf{x} for a finite (possibly large) value of n , when \mathbf{x} varies in phase space.

B. Reversibility error

We consider now the iteration of the map n times followed by the iterations of the inverse map still n times. Inserting a small additive noise at each forward and backward iteration, the final displacement with respect to the initial condition is a stochastic process,

whose variance defines the square on the reversibility error (RE). More precisely, letting $\mathbf{x}_{\varepsilon,0} = \mathbf{x}$ be the initial conditions, we consider the noisy orbit

$$\mathbf{x}_{\varepsilon,k} = M(\mathbf{x}_{\varepsilon,k-1}) + \varepsilon \xi_k, \quad \Xi_k = \lim_{\varepsilon \rightarrow 0} \frac{\mathbf{x}_{\varepsilon,k} - \mathbf{x}_k}{\varepsilon} \quad (19)$$

for $k = 1, \dots, n$. Starting from $\mathbf{x}_{\varepsilon,n}$ we consider the reversed noisy orbit

$$\begin{aligned} \mathbf{x}_{\varepsilon,n-k} &= M^{-1}(\mathbf{x}_{\varepsilon,n-k+1}) + \varepsilon \xi_{-k}, \\ \Xi_{n-k} &= \lim_{\varepsilon \rightarrow 0} \frac{\mathbf{x}_{\varepsilon,n-k} - \mathbf{x}_{n-k}}{\varepsilon}. \end{aligned} \quad (20)$$

The random vector Ξ_k satisfies a linear recurrence with initial condition $\Xi_0 = \mathbf{0}$, whereas Ξ_{n-k} satisfies another recurrence initialized by $\Xi_{n,0} = \Xi_n$ (see Refs. 27 and 28 for an explicit expression). We choose the random vectors ξ_k and $\xi_{-k'}$ independent for $k, k' > 0$,

$$\begin{aligned} \langle \xi_k \xi_{k'}^T \rangle &= \mathbf{I} \delta_{k,k'}, \quad \langle \xi_{-k} \xi_{-k'}^T \rangle = \mathbf{I} \delta_{k,k'}, \\ \langle \xi_{-k} \xi_{k'}^T \rangle &= \langle \xi_k \xi_{-k'}^T \rangle = 0. \end{aligned} \quad (21)$$

Letting $\Xi_{Rn} = \Xi_{n,-n}$ be the stochastic displacement with respect to the initial condition \mathbf{x} after reversing the orbit and $\Sigma_{Rn}^2(\mathbf{x})$ the corresponding covariance matrix, we define the reversibility error $E_R(\mathbf{x})$ according to

$$\begin{aligned} E_{Rn}^2(\mathbf{x}) &= \langle \Xi_{Rn} \cdot \Xi_{Rn} \rangle = \text{Tr}(\Sigma_{Rn}^2(\mathbf{x})), \\ \Sigma_{Rn}^2(\mathbf{x}) &= \langle \Xi_{Rn} \Xi_{Rn}^T \rangle. \end{aligned} \quad (22)$$

The covariance matrix that $\Sigma_{Rn}^2(\mathbf{x})$ can be expressed in terms of the tangent maps $DM^k(\mathbf{x})$ and their inverses $DM^{-k}(\mathbf{x})$. We do not quote their expression, which can be found in Refs. 26 and 27 since it can be proved²⁹ that for a symplectic map M in \mathbb{R}^{2d} , the error RE is related to LE by the following expression:

$$\begin{aligned} E_{Rn}^2(\mathbf{x}) &= E_{L_0}^2(\mathbf{x}) + E_{L_n}^2(\mathbf{x}) + 2 \sum_{k=1}^{n-1} E_{L_k}^2(\mathbf{x}), \\ E_{L_0}^2 &= \text{Tr}(\mathbf{I}) = 2d, \end{aligned} \quad (23)$$

or by the following recurrence starting with $n = 1$:

$$E_{Rn}^2 = E_{Rn-1}^2 + E_{L_n}^2 + E_{L_{n-1}}^2, \quad E_{R0}^2 = 0, \quad E_{L_0}^2 = 2d. \quad (24)$$

We finally define the reversibility error due to roundoff (REM). Letting $M_\varepsilon(\mathbf{x})$ the map computed with a finite precision ε (typically in the 8 bytes representation of reals $\varepsilon \simeq 10^{-17}$) and with M_ε^{-1} the inverse of M computed with finite accuracy, so that $M_\varepsilon^{-1}(M_\varepsilon(\mathbf{x})) \neq \mathbf{x}$, the modified reversibility error (REM) is defined according to

$$E_{\text{REM}n}(\mathbf{x}) = \frac{\|M_\varepsilon^{-n}(M_\varepsilon^n(\mathbf{x})) - \mathbf{x}\|}{\varepsilon}. \quad (25)$$

Letting $\mathbf{x}_{\varepsilon,n} = M_\varepsilon(\mathbf{x}_{\varepsilon,n-1})$ be the orbit computed with round off, the local error $(M_\varepsilon(\mathbf{x}_{\varepsilon,n-1}) - M(\mathbf{x}_{\varepsilon,n-1}))/\varepsilon$ is similar to a random vector, possibly correlated, if the map has a sufficiently high computational complexity (see Refs. 32 and 31). The difference with respect to the additive noise, we have considered to define RE, is that we have just a single realization. As a consequence, even though the behavior of RE and REM is similar, the last one exhibits large fluctuations, when n varies. On the other hand, the computation of REM

is really trivial since it requires a few lines of code, if the inverse map is available. This is the case of the reflection map for a waveguide. Indeed, to reverse the evolution after n iterations, we must simply change the sign of the horizontal velocity components(s) and iterate again the same map n times.

V. THE MODEL OF A 2D WAVEGUIDE

We present first a numerical analysis of the orbits for the map of the 2D waveguide where the corrugation is given by

$$f(x) = \cos(x). \tag{26}$$

The phase space coordinates are (x, v_x) and the map is defined on the cylinder $\mathbb{T}([-\pi, \pi]) \times [-1, 1]$, where $\mathbb{T}([-\pi, \pi])$ is the interval $[-\pi, \pi]$ with identified ends. The map has an elliptic fixed point at $x = 0, v_x = 0$, where $f(x)$ has a maximum and is approximated by $f(x) = 1 - \frac{1}{2}x^2 + O(x^4)$. We expand the map retaining only the linear terms in x, v_x . The first equation in (9) gives $\tau = 1 + \varepsilon$, neglecting second order terms in x and v_x . Since $f'(x) = -x + O(x^3)$ in the second equation, the square of f' is neglected and v_{zn} is replaced with 1. Accordingly, the second and third equations become

$$\begin{aligned} v_{xn+1} &= v_{xn} - 2\varepsilon(x_n + \tau v_{xn}), \\ x_{n+1} &= x_n + \tau(v_{xn} + v_{xn+1}). \end{aligned} \tag{27}$$

Letting $M(x) = Lx$ be the linear map, we have

$$L = \begin{pmatrix} 1 - 2\varepsilon\tau & 2\tau - 2\varepsilon\tau^2 \\ -2\varepsilon & 1 - 2\varepsilon\tau \end{pmatrix}, \tag{28}$$

so that $\det L = 1$ and $\frac{1}{2} \text{Tr} L = 1 - 2\varepsilon\tau$. The map is conjugated to a rotation $L = VR(\omega)V^{-1}$, where $\sin^2(\omega/2) = \tau\varepsilon = \varepsilon(1 + \varepsilon)$. In this case, we have $L_n = L^n$. Close to $x = 0$, the profile $z = 1 + \varepsilon - \varepsilon x^2/2$ is a concave mirror and the elliptical trajectories in phase space (x, v_x) correspond to caustics in configuration space, namely, the plane (x, z) where the rays propagate. Close to $x = \pi$, the profile is approximated by $z = 1 - \varepsilon + \frac{1}{2}\varepsilon(x - \pi)^2 + O(x - \pi)^4$ so that $\tau = 1 - \varepsilon$ and the linearized map is $(x_{n+1}, v_{xn+1})^T = L(x_n, v_{xn})^T$, where L is given by (27) with $\varepsilon \rightarrow -\varepsilon$. The map L is conjugated to a hyperbolic rotation $R_H(\alpha)$, where $\text{sh}^2(\alpha/2) = \varepsilon\tau = \varepsilon(1 - \varepsilon)$.

Near $x = \pi$, the waveguide corresponds to an optical system given by a plane and convex mirror.¹

The map defined by (9) was computed by solving the equation for τ with the bisection method initialized by $\tau_1 = 0.5/\sqrt{1 - v_{xn}^2}$ and $\tau_2 = 1.5/\sqrt{1 - v_{xn}^2}$. The convergence is achieved also when v_{xn} approaches 1 or -1 . The number of iterations to reach machine accuracy varies between 40 and 60. Newton's method is faster and machine accuracy is reached in less 10 iterations, but convergence problems are met when v_{xn} approaches 1 or -1 .

We have also computed the tangent map and the explicit expression is written in Appendix A. Writing the implicit equation $G(x_n, v_{xn}, \tau) = 0$, the solution is not defined if $\partial G/\partial \tau = 0$ a condition numerically never met. In Fig. 2, we compare the phase portraits with the color plots of LE, RE, and REM for the corrugation amplitude $\varepsilon = 0.1$ and orbits length $N = 200$. The correspondence is quite good and RE appears to be the smoothest indicator since it is free from oscillations and fluctuations when n varies. Increasing N does not change the plots significantly. Higher values of N are needed if

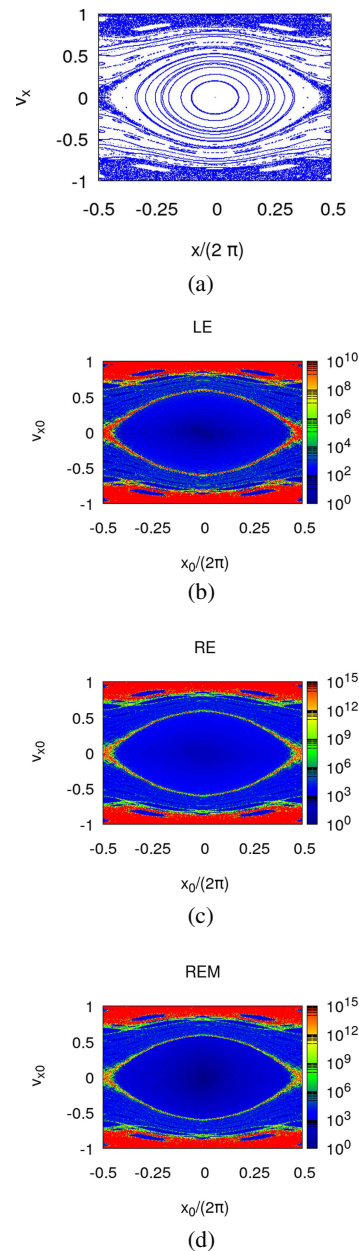


FIG. 2. From the top: (a) Phase portrait of the map for the 2D waveguide with corrugation $z = 1 + \varepsilon \cos(x)$ and $\varepsilon = 0.1$. (b) Color plot of LE for $N = 200$ iterations of the map. (c) Plot of RE for $N = 200$ iterations of the map. (d) Plot of REM for $N = 200$ iterations of the map.

one wishes to observe details in small regions where the transition from ordered to chaotic orbits occurs.

In Fig. 3, we compare the Lyapunov and reversibility indicators LE, RE, and REM for a single orbit of the reflection map with corrugation amplitude $\varepsilon = 0.1$ vs the iteration number n . The first

initial condition corresponds to a regular orbit and all the indicators for $n > 100$ follow a power law n^α with power $\alpha = 1$ for LE and $\alpha = 3/2$ for RE and REM. The second initial condition is at the boundary of the chaotic region. The third initial condition belongs to the chaotic region and the exponential rise is observed until saturation is reached. Indeed, in order to make a comparison with the 4D map, we have used the algorithm, where the derivatives are replaced with finite differences (the saturation occurs as long as the distance with the shadow orbit from the reference one is comparable with the diameter of the domain filled by the chaotic orbit). In Fig. 4 we compare the phase portraits with the color plots of LE, RE, and REM for corrugation amplitude $\varepsilon = 0.2$ and orbits length $N = 200$. Doubling the corrugation amplitude with respect to Fig. 2 determines a significant increase of the chaotic region, and a good correspondence between the phase portraits and the color plots of the Lyapunov and reversibility indicators LE, RE, and REM is found just as for the previous lower value of the corrugation amplitude.

VI. THE 3D MODEL

For the 3D waveguide, we choose the corrugated profile according to

$$f(x, y) = \cos x \cos y = \frac{1}{2} \cos(x + y) + \frac{1}{2} \cos(x - y). \quad (29)$$

We remark first that for initial conditions $y_0 = v_{y0} = 0$, we are back to the 2D case. If we choose $x_0 = y_0$ and $v_{x0} = v_{y0}$, the ray propagates in the $x = y$ plane as for the 2D waveguide. After a rotation of $\pi/4$, the ray propagates on the x', z plane where $x' = \sqrt{2} x$, $v_{x'} = \sqrt{2} v_x$, the corrugation function depends only on x' as $f = \frac{1}{2} [\cos(\sqrt{2} x') + 1]$ and its period is $\sqrt{2}\pi$.

When the ray does not propagate in a plane, the simplest case to analyze corresponds to the almost vertical propagation of the ray close to a critical point (x_c, y_c) of the corrugation function, where $\text{grad} f = 0$. The fixed point of the map $(x_c, y_c, v_x = 0, v_y = 0)$ is elliptic if f has a maximum at (x_c, y_c) and the corrugated surface near (x_c, y_c) behaves as a concave mirror.

If f has a minimum at (x_c, y_c) , then the surface behaves as a convex mirror and the critical point of the map is hyperbolic. For our model near $x = y = 0$, we have $f \simeq 1 - \frac{1}{2}(x^2 + y^2)$. The linearized map becomes

$$\begin{aligned} v_{xn+1} &= v_{xn} - 2\varepsilon(x_n + \tau v_{xn}), \\ x_{n+1} &= x_n + \tau(v_{xn} + v_{xn+1}), \\ v_{yn+1} &= v_{yn} - 2\varepsilon(y_n + \tau v_{yn}), \\ y_{n+1} &= y_n + \tau(v_{yn} + v_{yn+1}), \end{aligned} \quad (30)$$

where $\tau = 1 + \varepsilon$. Since τ is constant in this approximation, the maps in the (x, v_x) and (y, v_y) phase planes decouple and each of them is area preserving. The linear frequencies are equal and given by $\sin^2(\omega/2) = \varepsilon \tau$ as for the 2D case. The degeneracy can be removed choosing for instance $f(x, y) = \cos x + A \cos y$ with $A \neq 1$.

Near $x = 0, y = \pi$, we have $f \simeq 1 + \frac{1}{2}(x^2 + (y - \pi)^2)$ and the fixed point of the map is hyperbolic. More generally, $(0, 0)$, $(\pm\pi, \pm\pi)$, and $(\pm\pi, \mp\pi)$ are elliptic and $(0, \pm\pi)$ and

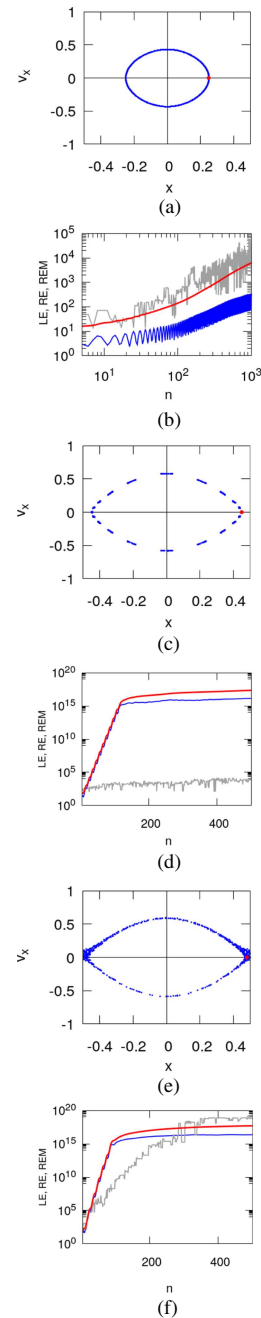


FIG. 3. Orbits of the 2D waveguide with $\varepsilon = 0.1$ for three different initial conditions $x_0/2\pi = 0.25, 0.45, 0.48$, and $v_x = 0$ [panels (a), (c), and (e), respectively] and corresponding indicators LE, RE, and REM vs n [panels (b), (d), and (f)].

$(\pm\pi, 0)$ are hyperbolic. We do not examine the projections of individual orbits on 2D phase space planes nor on 3D hyperplanes. Close to the elliptic fixed points, single 2D tori are recognizable in the projections on 3D hyperplanes and even 2D phase space planes, but the

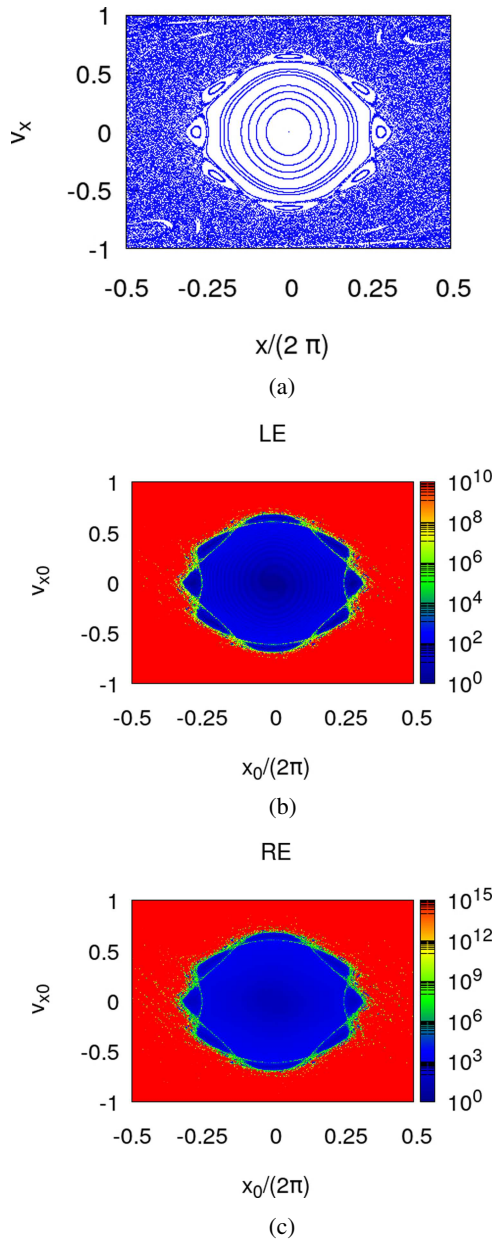


FIG. 4. From the top: (a) Phase portrait of the map for the 2D waveguide with corrugation $z = 1 + \varepsilon \cos(x)$ and $\varepsilon = 0.2$. (b) Color plot of LE for $N = 200$ iterations of the map. (c) Plot of RE for $N = 200$ iterations of the map.

projection of several orbits does not provide any useful information. For this reason, we show here the plots of our short term indicators LE, RE, and REM of orbits whose initial points belong to 2D phase planes.

The plots are obtained by computing our indicators for initial conditions $(x_0, v_{x0}, y_0, v_{y0})$ in a family of 2D phase planes, where

y_0 and v_{y0}/v_{x0} are kept fixed. Letting $v_{x0} = v_0 \cos(\phi_0)$ and $v_{y0} = v_0 \sin(\phi_0)$, we compare the errors for fixed values of y_0, ϕ_0 letting x_0, v_0 , which vary in $[-\pi, \pi] \times [-1, 1]$, where we choose a regular grid of $N_g \times N_g$ points. We have fixed the corrugation amplitude at $\varepsilon = 0.1$ because there is a good balance between regular and chaotic regions. We have computed LE by using the shadow orbit to evaluate the tangent map, namely, we have replaced the partial derivatives $\partial M_i / \partial x_j$ by finite differences, avoiding the cumbersome analytic evaluation. To this end, we have chosen four different initial conditions $\mathbf{x}_0 + \mathbf{e}_j \delta$ for $j \leq 4$ where \mathbf{e}_j are the orthonormal base vectors in \mathbb{R}^4 , namely, $(\mathbf{e}_j)_k = \delta_{jk}$. The tangent map is approximated by

$$DM^n(\mathbf{x}_0)\mathbf{e}_j \simeq \mathbf{w}_j(n) \equiv \frac{M^n(\mathbf{x}_0 + \mathbf{e}_j \delta) - M^n(\mathbf{x}_0)}{\delta}, \quad (31)$$

so that the Lyapunov error becomes

$$E_{Ln}^2 \simeq \sum_{j=1}^4 \|\mathbf{w}_j(n)\|^2. \quad (32)$$

The discrepancy is of order δ and the choice $\delta = 10^{-14}$ was made using double precision accuracy.

For $\phi_0 = 0$, we recover the plot computed with the tangent map for the 2D waveguide since the ray propagates in the x, z plane, but only if the sum in Eq. (32) runs only up to 2 (corresponding to the phase space coordinates to x, v_x). This is equivalent to defining LE by replacing DM^n with its first 2×2 block, which corresponds to tangent map for the 2D map. Indeed even though the orbits of the 2D and 4D map are the same for initial conditions $y_0 = v_{y0} = 0$, the components of 4D tangent map, not belonging the 2×2 block, are nonzero. On the contrary, REM does not change with respect to 2D map, because the (x, v_x) plane is invariant. To recover agreement between REM and RE, when LE is computed according to (32), which corresponds to the trace of $(DM^n)^T DM^n$, one can add a small random displacement of amplitude δ before reversing the orbit, in order to bring the orbit out of the invariant plane. When there is no invariant plane, the agreement between REM and RE is recovered without any random kick.

The regions of regular motion correspond to neighborhood of elliptic points of the resonant structures and the regions of chaotic motion to the separatrices joining the hyperbolic points. In addition the double resonances, due to single resonances intersection in action space, create other chaotic regions. The Fourier analysis might be used to classify the resonances because the resonant perturbation theory cannot be easily developed. In Fig. 5, we show the color plots of LE and RE for initial conditions in the (x, v_x) plane of LE and RE for corrugation amplitude $\varepsilon = 0.1$ choosing $\phi = 0$ and $y_0 = \pi/4$. The regions of regular motion correspond to the neighborhood of the elliptic points of resonances and the regions of chaotic motion to separatrices joining the hyperbolic points. In addition, the double resonances, due to single resonances intersection in action space, create other chaotic regions. The Fourier analysis might be used to classify the resonances, because, due to the nature of the reflection map, the perturbation methods used for the 2D and 4D standard like maps are difficult to implement. In Fig. 6, we show the projections on the (x, v_x) plane of the orbits with the same initial conditions in this plane as for the 2D map shown

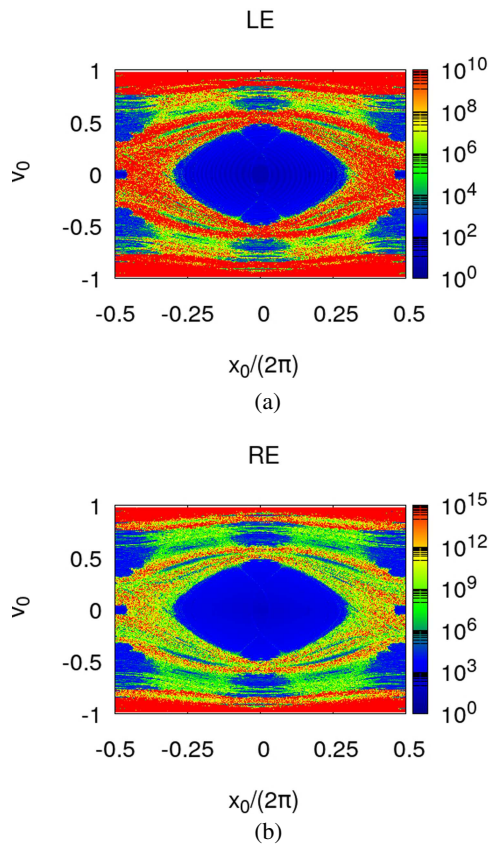


FIG. 5. From the top: (a) Plot of LE for the 4D reflection map of the 3D waveguide with corrugation amplitude $\varepsilon = 0.1$. The initial conditions $(x_0, y_0, v_{x0}, v_{y0})$ where $v_{x0} = v_0 \cos \phi_0$ and $v_{y0} = v_0 \sin \phi_0$, are chosen in a 2D plane obtained by keeping fixed $y_0 = \pi/4$ and $\phi_0 = 0$. The error LE is computed for $N = 200$ iterations of the map. We let (x_0, v_0) vary on a regular grid of $N_g \times N_g$ points, with $N_g = 200$, chosen in the rectangle $[-\pi, \pi] \times [-1, 1]$. (b) The same plot of RE.

in Fig. 3. The first frame shows clearly the projection on an orbit belonging to a torus \mathbb{T}^2 . Also, the remaining figures show the effect of the 2D projection of a 4D system. In Fig. 7, we show the color plots of LE and RE for initial conditions in the (x, v_x) plane and a higher value of the corrugation amplitude $\varepsilon = 0.2$ choosing $\phi = 0$ and $y_0 = \pi/2$.

VII. SHANNON CHANNEL CAPACITY

The possibility of computing fast stability indicators allows us to establish interesting properties that depend on them. Among others, in information theory, it is important to introduce the so called Shannon–Hartley channel capacity,

$$C = \lim_{t \rightarrow \infty} \frac{1}{t} \log_2 \left(\frac{Y}{X} \right), \tag{33}$$

where the time-dependent relation between input (X) and output (Y) describes the time evolution of the transfer process taking

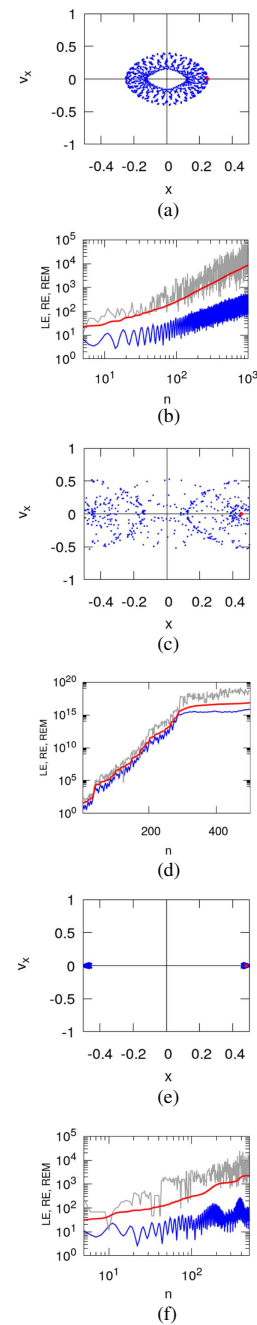


FIG. 6. Orbits of 4D waveguide with $\varepsilon = 0.1$ for initial conditions $x_0/2\pi = 0.25, 0.45, 0.48, y_0/2\pi = 0.125, v_0 = 0$ [panels (a), (c), and (e), respectively] and corresponding indicators LE, RE, and REM vs n [panels (b), (d), and (f)].

the message from transmitter to receiver. Equation (38) gives the maximum (ideal) information bit data-rate achievable in a physical system that carry electric signals/electromagnetic waves. In the high-frequency asymptotic, the propagation of waves through the

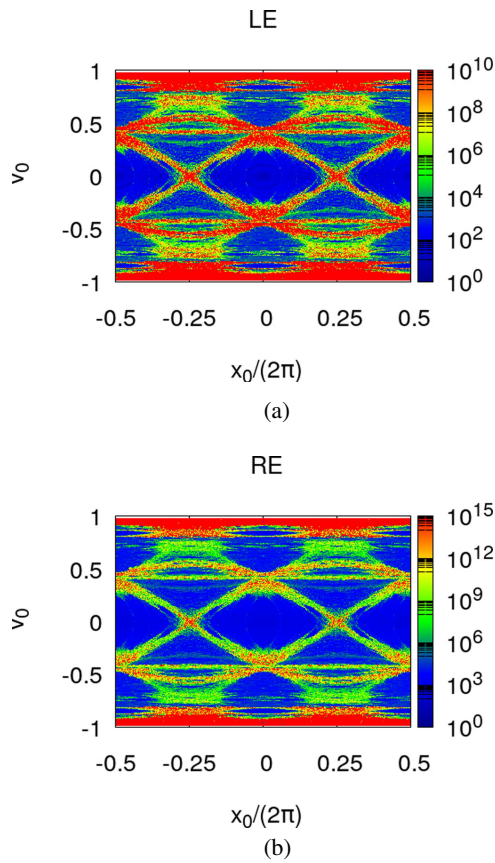


FIG. 7. Same plots as Fig. 6 for LE, RE, and REM for $\varepsilon = 0.1$ and fixed values of $y_0 = \pi/2$ and $\phi_0 = 0$. The number of iterations and grid points are the same $N = 200$, and $N_g = 200$.

corrugated channel in Fig. 1 has an isomorphism with classical ray trajectories underlying waves that bounce around the channel, given by the symplectic map (9). Therefore, one can think that the maximum Lyapunov exponent has an isomorphism with the Shannon–Hartley channel capacity. This has been recognized in Ref. 36 to be valid for any dynamical system and hence for a continuous time system. The relation between the channel capacity and the Lyapunov exponents of random matrices was first proposed by Ref. 37,

$$C = \lambda_1 = \lim_{t \rightarrow \infty} \frac{1}{t} \log E_L(t) = \lim_{t \rightarrow \infty} \frac{1}{t} \log E_R(t). \quad (34)$$

For recent works on the subject relating channel capacity to Lyapunov exponents and entropy (see Refs. 38 and 39). The use of the maximum Lyapunov exponent to capture the growing transfer impedance in linear chains of cascaded chaotic cavities has been used in Ref. 40. Consequently, fast dynamical indicators^{26,27} allow an estimation of the channel capacity. For a map like the waveguide map depending on one parameter ε , given a finite number of

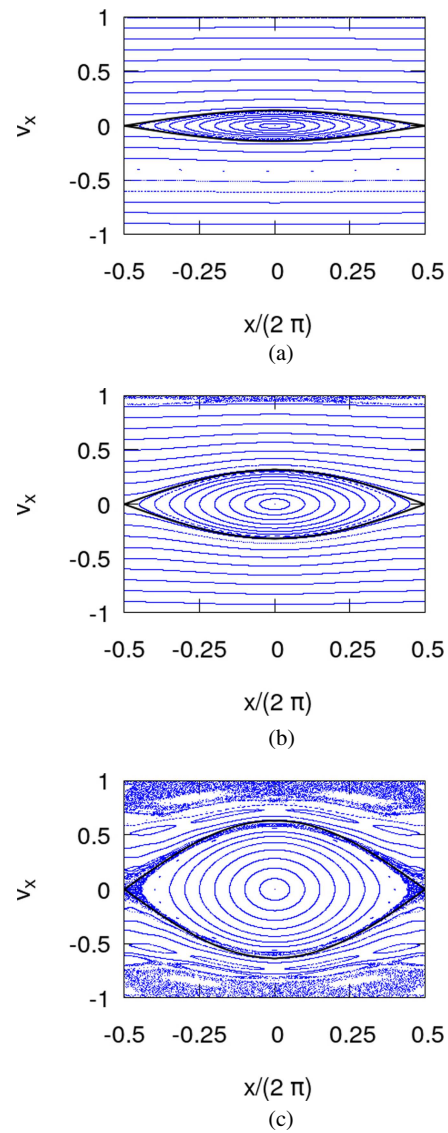


FIG. 8. Phase space portraits of the 2D map with the separatrix, black line, given by Eq. (38), for different values of the corrugation amplitude. Top frame: $\varepsilon = 0.005$. Center frame: $\varepsilon = 0.025$. Bottom frame: $\varepsilon = 0.1$.

iterations n , we introduce the sequences

$$\begin{aligned} C_{Ln}(\mathbf{x}, \varepsilon) &= \frac{1}{n} \log E_{Ln}(\mathbf{x}, \varepsilon), \\ C_{Rn}(\mathbf{x}, \varepsilon) &= \frac{1}{n} \log E_{Rn}(\mathbf{x}, \varepsilon), \end{aligned} \quad (35)$$

having the same limit $C(\mathbf{x}, \varepsilon)$ as $n \rightarrow \infty$. The channel capacities depend on the initial condition \mathbf{x} ; however, if \mathbf{x} belongs to an ergodic component, the result is the same for almost any choice of \mathbf{x} . For a parallel waveguide $\varepsilon = 0$, the channel capacities $C_{Ln}(\mathbf{x}, \varepsilon)$ and

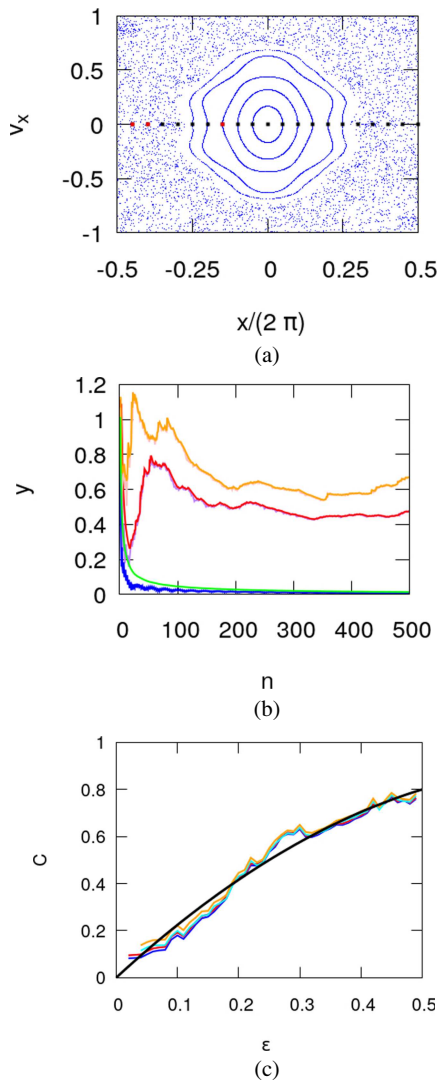


FIG. 9. Top panel: phase portrait of the 2D ray map for $\varepsilon = 0.25$. The blue and red dots correspond to the initial conditions. Middle panel: dependence on n of $C_{L_n}^L$ and $C_{R_n}^R$ for the chaotic orbits whose initial points are the first two red dots in left panel (LE pink, RE orange for the first orbit, LE purple, RE red for the second orbit) and the regular orbit whose initial point is the last red point (LE blue, RE green). Bottom panel: Growth of the average channel capacities (computed on a regular grid of 400×400 points) with ε for two values of n : C_{L_n} cyan for $n = 100$, blue for $n = 200$ and C_{R_n} , orange for $n = 100$. The black line is a quadratic fit given by Eq. (39).

$C_{L_n}(\mathbf{x}, \varepsilon)$ vanish asymptotically according to

$$\begin{aligned} C_{L_n}(\mathbf{x}, \varepsilon) &= \frac{1}{n} \log n + O(n^{-1}), \\ C_{R_n}(\mathbf{x}, \varepsilon) &= \frac{3}{2n} \log n + O(n^{-1}). \end{aligned} \tag{36}$$

For a corrugated waveguide, the phase plots of $C_{L_n}(\mathbf{x}, \varepsilon)$ and $C_{R_n}(\mathbf{x}, \varepsilon)$ for fixed n are of the same as the plot of E_{L_n} and E_{R_n} in a logarithmic scale shown in the Fig. 3 for the 2D waveguide and 6 for the 4D waveguide, up to the constant factor n^{-1} .

The 2D ray reflection map for $\varepsilon \ll 1$ is almost integrable and exhibits two distinct regions delimited by a separatrix, which can be approximated by

$$v_x = \pm 2\sqrt{\varepsilon} \cos\left(\frac{x}{2}\right) \tag{37}$$

(see Fig. 8). For $\varepsilon \sim 0.1$, the separatrix becomes a thin stochastic layer, whose area grows by further increasing ε . We have compared the dependence on n of the channel capacities $C_{L_n}(\mathbf{x}, \varepsilon)$ and $C_{R_n}(\mathbf{x}, \varepsilon)$ for one regular and two chaotic orbits (see Fig. 9). For the first orbit, the channel capacity vanishes as $n^{-1} \log n$, whereas for the last two chaotic orbits, a finite limit is approached.

In order to appreciate how the limit for $n \rightarrow \infty$ is reached and the dependence on the corrugated amplitude, we compute the following phase space averages [Fig. 9(c)]:

$$\begin{aligned} C_{L_n}(\varepsilon) &= \frac{1}{\mu_L(\mathcal{E})} \int_{\mathcal{E}} C_{L_n}(\mathbf{x}, \varepsilon) d\mathbf{x}, \\ C_{R_n}(\varepsilon) &= \frac{1}{\mu_L(\mathcal{E})} \int_{\mathcal{E}} C_{R_n}(\mathbf{x}, \varepsilon) d\mathbf{x}, \end{aligned} \tag{38}$$

where \mathcal{E} denotes the phase space and $\mu_L(\mathcal{E})$ its volume. We have analyzed the dependence on the corrugation amplitude ε of the average values of $C_{L_n}(\varepsilon)$ and $C_{R_n}(\varepsilon)$ for $n = 100$ and $n = 200$ [see Fig. 9 (bottom panel)]. The channel capacity varies almost monotonically from 0 to 0.8 and corresponds to the phase space average of the maximum Lyapunov exponent, since for $n = 200$ the asymptotic value appears to be reached. We have found the following quadratic fit with ε ,

$$C(\varepsilon) = 2.4\varepsilon - 1.6\varepsilon^2, \quad 0 \leq \varepsilon \leq \frac{1}{2}. \tag{39}$$

A similar analysis can be performed for the 4D map by computing the phase space average with a Monte Carlo sampling rather than on a regular grid as for the 2D map.

VIII. CONCLUSIONS

We have analyzed the propagation of a ray on 2D and 3D waveguide, given by two parallel lines or planes, one of which has a periodic corrugation. In both cases, the ray reflection maps on the uncorrugated line or plane are symplectic. The stability properties are relevant for the long term propagation of the rays. Indeed, in the chaotic regions, a diffusion occurs preventing the coherent propagation of a signal. We have analyzed the reflection maps using the short time indicators recently proposed: the Lyapunov error (LE), the reversibility errors (REs), and REM. The square of LE is the trace of the covariance matrix of the displacement, after n iterations of the map, induced by a small initial random displacement. The square of RE is the trace of the covariance matrix of the displacement from the initial condition, when the map is iterated forward and backward n times, adding at each step a small random displacement. Replacing the random displacement with the round off allows us to define a modified reversibility error REM, which is similar to RE,

though affected by large fluctuations due to the absence of averaging. In the 2D case, a good qualitative agreement with the phase portrait is found. For a fixed number n of reflections of the rays on the uncorrugated plane, all the indicators exhibit a similar behavior with a power law growth for regular orbits and exponential growth for chaotic orbits. For small corrugations, the motion is regular almost everywhere except in the neighborhood of the separatrix, occurring when the rays hit a minimum of the corrugated line or surface and for rays propagating almost parallel to the waveguide.

For the orbits of the 4D map, describing the ray dynamics of the 3D waveguide, LE and RE provide a satisfactory stability portrait, just as REM. A stability analysis in this case cannot be performed by looking at the projection of orbits on a 2D phase plane. Altogether these indicators quantify separately the effect of small initial displacements, additive noise and round off. The limited computational load and the simplicity of implementation of these indicators make them a convenient tool also for a parametric study of 2D and 3D waveguides. We have also considered the relation of our indicators with the channel capacity C . Indeed, the limit of $n^{-1} \log E_{L,n}$ and $n^{-1} \log E_{R,n}$ for $n \rightarrow \infty$ gives the maximum Lyapunov exponent, which is isomorphic to the channel capacity. The dependence on n for a given initial condition is consistent with theoretical estimates. The phase space average of the channel capacity is found to rise with the corrugation amplitude ε following a quadratic law.

ACKNOWLEDGMENTS

G. Gradoni wishes to acknowledge financial support of The Royal Society under Grant No. INF|R2|192066.

APPENDIX A: STABILITY OF EQUILIBRIA AND ORBITAL STABILITY

We recall the definitions of orbital stability to establish the correspondence with the frequently used terms such as regular, sticky, and chaotic orbits. The rigorous definitions of stability of an equilibrium point and of a trajectory for a deterministic dynamical systems data back to Lyapunov.³⁵ Given a continuous time dynamical system,

$$\frac{d}{dt} \mathbf{x}(t) = \Phi(\mathbf{x}(t)) \quad \mathbf{x} \in D \subset \mathbb{R}^d \quad \mathbf{x}(t) = S_t(\mathbf{x}) = e^{tD_\Phi} \mathbf{x}, \quad (A1)$$

where $\Phi(\mathbf{x}) : A \rightarrow \mathbb{R}^d$ is a smooth vector field, $D_\Phi = \sum_{i=1}^d \Phi(\mathbf{x}) \partial/\partial x_i$ is the Lie derivative and $K_t = e^{tD_\Phi}$ denotes the Koopmann evolution operator. An equilibrium point \mathbf{x}_c defined by $\Phi(\mathbf{x}_c) = 0$ is (Lyapunov) stable if to any $\mathbf{x}_0 \in A$ and $\varepsilon > 0$ such that $B_\varepsilon(\mathbf{x}_0) \in A$, we can associate $0 < r(\varepsilon) \leq \varepsilon$ continuous with $r(0) = 0$ such that

$$\|\mathbf{x}_0 - \mathbf{x}_c\| < \varepsilon \implies \|\mathbf{x}(t) - \mathbf{x}_c\| < r(\varepsilon), \quad \forall t > 0. \quad (A2)$$

If in addition $\lim_{t \rightarrow +\infty} \mathbf{x}(t) \rightarrow \mathbf{x}_c$, then \mathbf{x}_c is stable and attractive or according to Lyapunov asymptotically stable. If $\|\mathbf{x}(t) - \mathbf{x}_c\| < C\|\mathbf{x}_0 - \mathbf{x}_c\| e^{-\lambda t} \forall t > 0$, the point is exponentially stable. Such a condition is fulfilled if $\Phi(\mathbf{x})$ is a real analytic function in a poly-disk centered at \mathbf{x}_c and its linear part is $A(\mathbf{x} - \mathbf{x}_c)$ and the spectrum of the matrix A is in the half plane $Re(z) \leq -\lambda < 0$. Indeed, in this case, the Poincaré Dulac theorem ensures the existence of an analytic linearizing diffeomorphism.

Let $A \subset \mathbb{R}^d$ be any invariant set $S_t(A) = A$. The orbit $\mathbf{x}(t) \equiv S_t(\mathbf{x})$ issued at $t = 0$ from any $\mathbf{x} \in A$ such $B_\varepsilon(\mathbf{x}) \subset A$ is stable for $\forall \varepsilon \ll 1$ if the orbit $\mathbf{y}(t) \equiv S_t(\mathbf{y})$ issued from a point \mathbf{y} sufficiently close to \mathbf{x} , namely, remains for any $t > 0$ close to the orbit issued from \mathbf{x} , namely, to any $\varepsilon > 0$, we can associate a $r(\varepsilon) > 0$ such that

$$\|\mathbf{y} - \mathbf{x}\| < \varepsilon \implies \|\mathbf{y}(t) - \mathbf{x}(t)\| < r(\varepsilon) \quad \forall t > 0. \quad (A3)$$

If in addition $S_t(\mathbf{x})$ is asymptotically dense on a set $\mathcal{A} \subset A$, namely, $\lim_{t \rightarrow \infty} d(S_t(\mathbf{x}), \mathcal{A}) = 0$, then the orbit is stable being asymptotically attracted by the attractor \mathcal{A} . Typical examples are the stable cycles and the stable attracting tori \mathbb{T}^k with $k < d$.

This is the rigorous definition of orbital stability according to Lyapunov. To any invariant subset $A \subset \mathbb{R}^d$ where the orbital stability is fulfilled, one usually refers as stable region or region of regular orbits. Any other invariant compact subset $B \subset \mathbb{R}^d$ where $\|\mathbf{y}(t) - \mathbf{x}(t)\|/\|\mathbf{y} - \mathbf{x}\|$ have an asymptotic exponential growth with t for $\mathbf{y} \rightarrow \mathbf{x}$, is called chaotic, since the orbits stretch and fold.

To conclude, the Lyapunov stable orbits are called *regular* or *stable*. The unstable orbits with exponential divergence in compact invariant domains are called *chaotic* or *unstable*.

The extension of these definitions to maps $M(\mathbf{x}) = K\mathbf{x}$, from an open set $A \subset \mathbb{R}^d$ into \mathbb{R}^d , where K is Koopmann operator, is obvious. The continuous orbit $\mathbf{x}(t) = S_t(\mathbf{x}) = K_t \mathbf{x}$ is replaced by the discrete orbit provided by $\mathbf{x}_n = M^n(\mathbf{x}) = K^n \mathbf{x}$ or by the recurrence $\mathbf{x}_n = M(\mathbf{x}_{n-1}) = K \mathbf{x}_{n-1}$. The symplectic maps in \mathbb{R}^{2m} is particular since there are no attracting points, $d = 2m$ is even, the volumes in \mathbb{R}^{2m} are preserved just as the even dimensional Poincaré parallelotopes with $2k$ edges with $1 < k \leq m$.

APPENDIX B: TANGENT MAP FOR 2D WAVEGUIDE

The equation that determines $\tau(x, v)$ is

$$G(x, v, \tau) = 1 + \varepsilon f(x + \tau v) - \tau \sqrt{1 - v^2} = 0, \quad (B1)$$

$$\frac{\partial \tau}{\partial x} = -\frac{\frac{\partial G}{\partial x}}{\frac{\partial G}{\partial \tau}} = \frac{\varepsilon f'}{\sqrt{1 - v^2} - \varepsilon v f'},$$

$$\frac{\partial \tau}{\partial v} = -\frac{\frac{\partial G}{\partial v}}{\frac{\partial G}{\partial \tau}} = \frac{\varepsilon \tau f' + \tau v / \sqrt{1 - v^2}}{\sqrt{1 - v^2} - \varepsilon v f'}.$$

Letting $v_x = \cos \theta \equiv v$ and $v_z = \sin \theta \equiv \sqrt{1 - v^2}$ the recurrence which determines the symplectic map $M = (x, v)$ is given by

$$G(x_n, v_n, \tau) = 0, \quad (B2)$$

$$v_{n+1} = v_n - 2 \frac{\varepsilon^2 f'^2 v_n - \varepsilon f' \sqrt{1 - v_n^2}}{1 + \varepsilon^2 f'^2},$$

$$x_{n+1} = x_n + \tau v_n + \tau \frac{\sqrt{1 - v_n^2}}{\sqrt{1 - v_{n+1}^2}} v_{n+1}.$$

The tangent map is given by

$$\begin{aligned} \frac{\partial v_{n+1}}{\partial x_n} &= \frac{2\varepsilon f''}{(1 + \varepsilon^2 f'^2)^2} \left[-2\varepsilon v_n f' + \sqrt{1 - v_n^2} (1 - \varepsilon^2 f'^2) \right] \\ &\quad \times \left(1 + v_n \frac{\partial \tau}{\partial x_n} \right), \\ \frac{\partial v_{n+1}}{\partial v_n} &= 1 - \frac{2\varepsilon f'}{1 + \varepsilon^2 f'^2} \left(\varepsilon f' + \frac{v_n}{\sqrt{1 - v_n^2}} \right) \\ &\quad + \frac{2\varepsilon f''}{(1 + \varepsilon^2 f'^2)^2} \left[-2\varepsilon v_n f' + \sqrt{1 - v_n^2} (1 - \varepsilon^2 f'^2) \right] \\ &\quad \times \left(\tau + v_n \frac{\partial \tau}{\partial v_n} \right), \\ \frac{\partial x_{n+1}}{\partial x_n} &= 1 + \left(v_n + v_{n+1} \frac{\sqrt{1 - v_n^2}}{\sqrt{1 - v_{n+1}^2}} \right) \frac{\partial \tau}{\partial x_n} \\ &\quad + \tau \frac{\sqrt{1 - v_n^2}}{(1 - v_{n+1}^2)^{3/2}} \frac{\partial v_{n+1}}{\partial x_n}, \\ \frac{\partial x_{n+1}}{\partial v_n} &= \tau + \left(v_n + v_{n+1} \frac{\sqrt{1 - v_n^2}}{\sqrt{1 - v_{n+1}^2}} \right) \frac{\partial \tau}{\partial v_n} \\ &\quad + \tau \frac{\sqrt{1 - v_n^2}}{(1 - v_{n+1}^2)^{3/2}} \frac{\partial v_{n+1}}{\partial v_n} \\ &\quad - \tau \frac{v_n}{\sqrt{1 - v_n^2}} \frac{v_{n+1}}{\sqrt{1 - v_{n+1}^2}}. \end{aligned} \tag{B3}$$

In all the previous formulas, $f = f(x_n + \tau v_n)$ with $f' = f'(x_n + \tau v_n)$ and $f'' = f''(x_n + \tau v_n)$.

In order to check the limit $\varepsilon \rightarrow 0$, we recall that the map is given by

$$\begin{aligned} \tau \sqrt{1 - v_n^2} &= 1, \quad v_{n+1} = v_n, \\ x_{n+1} &= x_n + 2 \frac{v_n}{\sqrt{1 - v_n^2}}. \end{aligned} \tag{B4}$$

In this case, the tangent map is given by

$$\begin{aligned} \frac{\partial x_{n+1}}{\partial x_n} &= 1, \\ \frac{\partial x_{n+1}}{\partial v_n} &= \frac{2}{(1 - v_n^2)^{3/2}}, \\ \frac{\partial v_{n+1}}{\partial x_n} &= 0, \\ \frac{\partial v_{n+1}}{\partial v_n} &= 1. \end{aligned} \tag{B5}$$

In our example, we choose $f(x)$ periodic of period 2π and scale the coordinates according to $x = 2\pi x'$ so that the new tangent map is

given by

$$\begin{aligned} \frac{\partial x'_{n+1}}{\partial x'_n} &= \frac{\partial x_{n+1}}{\partial x_n}, \\ \frac{\partial x'_{n+1}}{\partial v_n} &= \frac{1}{2\pi} \frac{\partial x_{n+1}}{\partial v_n}, \\ \frac{\partial v_{n+1}}{\partial x'_n} &= 2\pi \frac{\partial v_{n+1}}{\partial x_n}. \end{aligned} \tag{B6}$$

APPENDIX C: THE 3D WAVEGUIDE

The equation for the corrugates waveguide is given by Eq. (12), where $f(x, y)$ is a periodic function. The normal vector \mathbf{v} and the tangent vectors $\boldsymbol{\tau}_x, \boldsymbol{\tau}_y$ are given by

$$\begin{aligned} \mathbf{v}(x, y) &= \frac{(\varepsilon f_x, \varepsilon f_y, -1)^T}{\sqrt{1 + \varepsilon^2 (f_x^2 + f_y^2)}}, \\ \boldsymbol{\tau}_x &= \frac{(1, 0, \varepsilon f_x)^T}{\sqrt{1 + \varepsilon^2 f_x^2}}, \\ \boldsymbol{\tau}_y &= \frac{(0, 1, \varepsilon f_y)^T}{\sqrt{1 + \varepsilon^2 f_y^2}}, \end{aligned} \tag{C1}$$

where $f_x \equiv \partial f / \partial x$ and $f_y \equiv \partial f / \partial y$. For an analogy with the 2D case, we might introduce the curvilinear abscissas s_x, s_y on the lines on the corrugated plane having y fixed and x fixed, respectively,

$$\begin{aligned} s_x(x, y) &= \int_0^x \sqrt{1 + \varepsilon^2 f_x^2(x', y)} dx', \\ s_y(x, y) &= \int_0^y \sqrt{1 + \varepsilon^2 f_y^2(x, y')} dy', \end{aligned} \tag{C2}$$

so that, keeping y fixed, $ds_x = \sqrt{1 + \varepsilon^2 f_x^2(x, y)} dx$ and, keeping x fixed, $ds_y = \sqrt{1 + \varepsilon^2 f_y^2(x, y)} dy$. The transformation from (x, y) to (s_x, s_y) is invertible. Letting $P_0 = (x_0, y_0, 0)$ be a point on the plane, $Q = (x, y, z(x, y))$ a point on the corrugated plane, and $P_1 = (x_1, y_1, 0)$ a new point on the plane we consider a ray whose path is P_0, Q, P_1 . We denote with \mathbf{v}_0 and \mathbf{v} the velocity of the ray directed from P_0 to Q and from Q to P_1 . As for the 2D case, we keep P_0 and P_1 fixed letting Q vary and consider the ray path length H , which depends on Q ,

$$\begin{aligned} H(x, y) &= h(x_0, y_0, x, y) + h(x_1, y_1, x, y), \\ h(x_0, y_0, x, y) &= \sqrt{(x - x_0)^2 + (y - y_0)^2 + (1 + \varepsilon f(x, y))^2}. \end{aligned} \tag{C3}$$

The velocities \mathbf{v}_0 and \mathbf{v} , denoting for brevity $h_0 \equiv h(x_0, y_0, x, y)$ and $h_1 \equiv h(x_1, y_1, x, y)$, are given by

$$\begin{aligned} \mathbf{v}_0 &= \frac{(x - x_0, y - y_0, 1 + \varepsilon f(x, y))^T}{h(x_0, y_0, x, y)}, \\ \mathbf{v} &= \frac{(x_1 - x_0, y_1 - y_0, 1 + \varepsilon f(x, y))^T}{h(x_1, y_1, x, y)}. \end{aligned} \tag{C4}$$

We first compute the derivatives of h_0 and h_1 with respect to x and y ,

$$\begin{aligned}\frac{\partial}{\partial x} h_0 &= \frac{x - x_0 + (1 + \varepsilon f) \varepsilon f_x}{h_0} = \mathbf{v}_0 \cdot \boldsymbol{\tau}_x \sqrt{1 + \varepsilon^2 f_x^2}, \\ \frac{\partial}{\partial y} h_0 &= \frac{y - y_0 + (1 + \varepsilon f) \varepsilon f_y}{h_0} = \mathbf{v}_0 \cdot \boldsymbol{\tau}_y \sqrt{1 + \varepsilon^2 f_y^2}, \\ \frac{\partial}{\partial x} h_1 &= \frac{x - x_1 + (1 + \varepsilon f) \varepsilon f_x}{h_1} = -\mathbf{v} \cdot \boldsymbol{\tau}_x \sqrt{1 + \varepsilon^2 f_x^2}, \\ \frac{\partial}{\partial y} h_1 &= \frac{y - y_1 + (1 + \varepsilon f) \varepsilon f_y}{h_1} = -\mathbf{v} \cdot \boldsymbol{\tau}_y \sqrt{1 + \varepsilon^2 f_y^2}.\end{aligned}\quad (\text{C5})$$

Choosing h_0 and h_1 a functions of s_x, s_y rather than x, y one has $\partial h_0 / \partial s_\alpha = \mathbf{v}_0 \cdot \boldsymbol{\tau}_\alpha$ and $\partial h_1 / \partial s_\alpha = -\mathbf{v} \cdot \boldsymbol{\tau}_\alpha$ for $\alpha = x, y$. The function H is stationary when $\mathbf{v}_0 \cdot \boldsymbol{\tau}_x = \mathbf{v}_0 \cdot \boldsymbol{\tau}_x$ and $\mathbf{v}_0 \cdot \boldsymbol{\tau}_y = \mathbf{v}_0 \cdot \boldsymbol{\tau}_y$, namely, when the projection on the tangent plane of the incoming and outgoing ray velocities are equal. This corresponds to the reflection condition since the normal components of \mathbf{v}_0 and \mathbf{v} are opposite. The derivatives with respect to x_0, y_0 and x_1, y_1 are given by

$$\begin{aligned}\frac{\partial h_0}{\partial x_0} &= \frac{x_0 - x}{h_0} = -v_{x0}, & \frac{\partial h_0}{\partial y_0} &= \frac{y_0 - y}{h_0} = -v_{y0}, \\ \frac{\partial h_1}{\partial x_1} &= \frac{x_1 - x}{h_1} = v_{x1}, & \frac{\partial h_1}{\partial y_1} &= \frac{y_1 - y}{h_1} = -v_{y1}.\end{aligned}\quad (\text{C6})$$

Finally, letting (x_*, y_*) the point where H is stationary and which depends on end points (x_0, y_0) and (x_1, y_1) , we introduce the function F defined as the value of H evaluated at the stationary point and compute its differential

$$\begin{aligned}F(x_0, y_0, x_1, y_1) &= h(x_0, y_0, x_*, y_*) + h(x_1, y_1, x_*, y_*), \\ dF &= -v_{x0} dx_0 - v_{y0} dy_0 + v_{x1} dx_1 + v_{y1} dy_1.\end{aligned}\quad (\text{C7})$$

As a consequence, F is the generating function of a canonical transformation M , which maps $(x_0, v_{x0}, y_0, v_{y0})$ into $(x_1, v_{x1}, y_1, v_{y1})$. Denoting with $\mathbf{x}_n = (x_n, v_{xn}, y_n, v_{yn})^T$ the phase space point reached after n iterations of the symplectic map M , the recurrence from \mathbf{x}_n to \mathbf{x}_{n+1} is obtained first by computing the transit time τ from $P_n = (x_n, y_n)$ to the point $Q = (x_*, y_*)$ on the corrugated surface. Then, we notice that the horizontal plane projections of the velocities $\mathbf{v}_* = \mathbf{v}_n - 2\mathbf{v}(\mathbf{v}_n \cdot \mathbf{v})$ and \mathbf{v}_{n+1} of the ray reflected at Q and $P_{n+1} = (x_{n+1}, y_{n+1})$ are equal. Finally, we determine the displacement from P_n to P_{n+1} . The equations defining the recurrence from \mathbf{x}_n to \mathbf{x}_{n+1} are given by (14).

DATA AVAILABILITY

The data that support the findings of this study are openly available in <https://github.com/gabrielegradoni/WaveguideStability>, Ref. 41.

REFERENCES

¹A. Bazzani, P. Freguglia, and G. Turchetti, "Hamiltonian analytical optics and simulations of betatronic motion by optical devices," in *Nonlinear Dynamics and Collective Effects in Particle Beam Physics* (World Scientific, 2019), pp. 23–46.

²N. Chernov and M. Markarian, "Chaotic billiards," in *Mathematical Surveys and Monographs*, American Mathematical Society Vol. 127 (2006), see <https://www.ams.org/books/surv/127/>.

³L. A. Bunimovich, "On the ergodic properties of nowhere dispersing billiards," *Commun. Math. Phys.* **65**(3), 295–312 (1979).

⁴J. Redmond and S. Tabachnikov, "Introducing symplectic billiards," see <https://www.math.psu.edu/tabachni/prints/Notes5.pdf>.

⁵S. Tabachnikov, "Billiards," see <https://www.math.psu.edu/tabachni/Books/billiardsbook.pdf>.

⁶S. Woo Park, "An introduction to dynamical billiards," see <https://math.uchicago.edu/may/REU2014/REUPapers/Park.pdf>.

⁷K. M. Frahm and D. L. Shepelyansky, "Quantum localization in rough billiards," *Phys. Rev. Lett.* **78**, 1440 (1997).

⁸F. Borgonovi, G. Casati, and B. Li, "Diffusion and localization in chaotic billiards," *Phys. Rev. Lett.* **77**, 23 (1996), see <https://arxiv.org/pdf/cond-mat/9610158.pdf>.

⁹D. Holm and G. Kovacic, "Homoclinic chaos for ray optics in a fiber," *Physica D* **51**, 177 (1991).

¹⁰S. S. Abdullaev and G. M. Zaslavskii, "Classical nonlinear dynamics and chaos of rays in problems of wave propagation in inhomogeneous media," *Usp. Fiz. Nauk.* **161**, 1 (1991).

¹¹D. Douglas, "Chaotic billiard lasers," *Nature* **465**, 696 (2010).

¹²S. Creagh, "Directional emission from weakly eccentric resonators," *Phys. Rev. Lett.* **98**, 153901 (2007).

¹³G. Tanner, "Dynamical energy analysis determining wave energy distributions in vibro-acoustical structures in the high-frequency regime," *J. Sound Vib.* **320**(4), 1023–1038 (2009).

¹⁴E. Leonel, D. da Costa, and C. Dettmann, "Scaling invariance for the escape of particles from a periodically corrugated waveguide," *Phys. Lett. A* **376**, 421 (2012).

¹⁵J. de Oliveira, C. Dettmann, D. da Costa, and E. Leonel, "Scaling invariance of the diffusion coefficient in a family of two-dimensional Hamiltonian mappings," *Phys. Rev. E* **87**, 062904 (2013).

¹⁶G. Gradoni, J.-H. Yeh, B. Xiao, T. Antonsen, S. Anlage, and E. Ott, "Predicting the statistics of wave transport through chaotic cavities by the random coupling model: A review and recent progress," *Wave Motion* **51**, 606 (2014).

¹⁷G. Forte, F. Cecconi, and A. Vulpiani, "Transport and fluctuation-dissipation relations in asymptotic and preasymptotic diffusion across channels with variable section," *Phys. Rev. E* **90**, 062110 (2014), see http://denali.phys.uniroma1.it/cecconi/MyPapersPDF/gforte_PRE90.pdf.

¹⁸F. Cecconi, V. Blakaj, G. Gradoni, and A. Vulpiani, "Diffusive transport in highly corrugated channels," *Phys. Lett. A* **383**, 1084–1091 (2018).

¹⁹C. Froeschlé and E. Lega, "On the structure of symplectic mappings. The fast Lyapunov indicator: A very sensitive tool," *Celestial Mech. Dyn. Astron.* **78**, 167–195 (2000).

²⁰C. Froeschlé, M. Guzzo, and E. Lega, "Graphical evolution of the Arnold web: From order to chaos," *Science* **289**, 2108–2110 (2000).

²¹C. Skokos, T. Bountis, and C. Antonopoulos, "Geometrical properties of local dynamics in Hamiltonian systems: The generalized alignment index (GALI) method," *Physica D* **231**, 3054 (2007).

²²N. P. Maffione, L. A. Darriba, P. M. Cincotta, and C. M. Giordano, "Comparison of different indicators of chaos based on the deviation vectors. Application to symplectic mappings," *Celestial Mech. Dyn. Astron.* **111**, 285–307 (2011), see <https://arxiv.org/abs/1108.2196>.

²³N. P. Maffione, L. A. Darriba, P. M. Cincotta, and C. M. Giordano, "Comparative study of variational chaos indicators and ODEs numerical integrators," *Int. J. Bifurcation Chaos* **22**, 1230033 (2012).

²⁴D. Ruelle, "An inequality for the entropy of differentiable maps," *Bol. Soc. Bras. Mat.* **9**, 83–87 (1978).

²⁵A. Roy, T. Downarowicz, T. Downarowicz, and M. Misiurewicz, "Topological entropy," see http://www.scholarpedia.org/article/Topological_entropy#Mean_topological_dimension.

²⁶F. Panichi, L. Ciotti, and G. Turchetti, "Fidelity and reversibility in the restricted three body problem," *Commun. Nonlinear Sci. Numer. Simul.* **35**, 53 (2015).

- ²⁷F. Panichi, K. Goździewski, and G. Turchetti, “The reversibility error method (REM): A new, dynamical fast indicator for planetary dynamics,” *MNRAS* **468**, 469 (2017).
- ²⁸F. Panichi and G. Turchetti, “Fast indicators of orbital stability: A survey on Lyapunov and reversibility errors,” in *Progress in Relativity* (InTechOpen, 2020), pp. 1–21; see <https://www.intechopen.com/online-first/fast-indicators-for-orbital-stability-a-survey-on-lyapunov-and-reversibility-errors>.
- ²⁹G. Turchetti and F. Panichi “Fast Lyapunov and reversibility error invariant indicators,” *Phys. Rev. E* (submitted).
- ³⁰D. Faranda, M. F. Mestre, and G. Turchetti, “Analysis of round off errors with reversibility test as a dynamical indicator,” *Int. J. Bifurcation Chaos* **22**, 1250215 (2012).
- ³¹G. Turchetti, S. Vaienti, and F. Zanlungo, “Asymptotic distribution of global errors in the numerical computations of dynamical systems,” *Physica A* **389**, 4994–5006 (2010).
- ³²E. Hairer, C. Lubich, and G. Wanner, *Geometric Numerical Integration: Structure-Preserving Algorithms for Ordinary Differential Equations*, 2nd ed. (Springer, Dordrecht, 2006).
- ³³G. Turchetti and F. Panichi, “Birkhoff normal forms and stability indicators for betatronic motion,” in *Proceedings of the NOCE Workshop, Arcidosso, September 2017*, edited by S. Di Mitri, S. Chattopadhyay, and M. Cornacchia (World Scientific, 2019).
- ³⁴V. I. Oseledets, “A multiplicative ergodic theorem. Characteristic Lyapunov exponents of dynamical systems,” *Trudy Mosk. Mat. Obs.* **19**, 179–210 (1968) [*Trans. Moscow Math. Soc.* **19**, 197–231 (1968)].
- ³⁵A. M. Lyapunov, “The general problem of the stability of motion,” Doctoral dissertation in Russian (1892). English translation *Stability of Motion* (Academic Press, New York, 1966).
- ³⁶*Isomorphism between Maximum Lyapunov Exponent and Shannon’s Channel Capacity*, edited by G. Friedland and A. Metere, see <https://arxiv.org/pdf/1706.08638.pdf> (2018).
- ³⁷T. Holliday, A. Goldsmith, and P. W. Glynn, “Capacity of finite state channels based on Lyapunov exponents of random matrices,” *IEEE Trans. Inf. Theor.* **52**(8), 3509–3532 (2006).
- ³⁸T. Holliday, P. Glynn, and A. Goldsmith, “On entropy and Lyapunov exponents for finite-state channels,” see <http://www.yaroslavvb.com/papers/holliday-entropy.pdf>.
- ³⁹J. M. Ebeid, “Relating information theoretic limits to the Lyapunov exponents of a dynamical system,” see https://www.ideals.illinois.edu/bitstream/handle/2142/16882/Ebeid_Hani-James.pdf?sequence=1&isAllowed=y.
- ⁴⁰G. Gradoni, T. Antonsen, and E. Ott, “Impedance and power fluctuations in linear chains of coupled wave chaotic cavities,” *Phys. Rev. E* **86**(4), 046204 (2012).
- ⁴¹G. Gradoni, G. Turchetti, and F. Panichi, “Propagation of rays in corrugated waveguides,” *Software Impacts* (2021).